High Density Hydroxyl Anions in a Microporous Crystal: $[Ca_{24}Al_{28}O_{64}]^{4+}\cdot 4(OH^-)$

Jiang Li,[†] Fan Huang,[†] Lian Wang,[†] Shu Qin Yu,[†] Youshifumi Torimoto,[‡] Masayoshi Sadakata,[‡] and Quan Xin Li*,[†]

Department of Chemical Physics, Lab of Biomass Clean Energy, University of Science & Technology of China, Hefei, Anhui, 230026, People's Republic of China, and Department of Chemical System Engineering, School of Engineering, The University of Tokyo, 7-3-1 Hongo, Bunkyo-ku, Tokyo 113-8656, Japan

Received January 7, 2005. Revised Manuscript Received March 17, 2005

By retreating the C12A7-O^- microporous crystal ($[Ca_{24}Al_{28}O_{64}]^{4+}\cdot 4O^-$) in a high-temperature (1350 °C) and water vapor environment, almost 100% O^- and O_2^- anions in C12A7-O^- have been substituted by the OH^- anions, leading to the formation of a high-intensity OH^- emission material, $[Ca_{24}Al_{28}O_{64}]^{4+}\cdot 4OH^-$ (C12A7-OH^-). The formation of OH^- in C12A7-OH^- was identified by investigating the anionic species both on the surface and in the bulk as well as its emission features with Fourier-transform IR absorption, electron paramagnetic resonance, and time-of-flight mass spectra. The concentration of OH^- anions in C12A7-OH^- is estimated to be more than 7×10^{20} cm^{-3}. Furthermore, a sustainable and stable OH^- emission current of 11.7 $\mu A/cm^2$ from C12A7-OH^- has been obtained at a sample surface temperature of 780 °C under an extraction field of 1300 V/cm. The emission features of C12A7-OH^-, such as temperature and field effects, have been also investigated. It is expected that the present material could be practically used as an OH^- anions storage and generator.

1. Introduction

There has been great concern of OH^- in ionic oxide crystals in the past decades.[1−12] When the ionic oxides are exposed to the UV irradiation or γ irradiation in the presence of adsorbing H_2 or H_2O, the vacancies of the ionic oxides will be occupied by the OH^- anions with the $Fs^+(H)$ or V^-_{OH} color centers generating at the surface of the crystals.[1−10] By exposition of these crystals to irradiation and alkanes, the color centers containing OH^- anions are also generated.[11,12] However, the concentration of OH^- anions formed by exposing UV irradiation or γ irradiation onto the surfaces, generally, is low in the above crystals .[6,7] To obtain strong OH^- anion emission, it needs to find a new material which can trap a high-concentration OH^- anions in the body.

Recently, there have been great interests in the emission characteristic and various applications of a microporous crystal $12CaO\cdot 7Al_2O_3$ (C12A7).[13−22] The structure of C12A7 which contains two molecules per unit cell is characterized by a positively charged lattice framework $[Ca_{24}Al_{28}O_{64}]^{4+}$ including 12 sub-nanometer-sized cages with a free space of about 0.4 nm in diameter. The remaining two oxide ions (O^{2-}) are clathrated in the cages, and the positive charge concentration in the lattice framework gives a theoretical maximum of 2.3×10^{21} cm^{-3} monovalent anions.[17] Otherwise, it has been reported that O^{2-} in C12A7 cages can be substituted by X^- ($X^- = F^-$, Cl^-), O^-, H^-, and electrons to form the derivatives $[Ca_{24}Al_{28}O_{64}]^{4+}\cdot 4(X^-)$,[23] $[Ca_{24}Al_{28}O_{64}]^{4+}\cdot 4(O^-)$[17] (defined as C12A7-$O^-$), $[Ca_{24}Al_{28}O_{64}]^{4+}\cdot 4(H^-)$[16], and

* To whom correspondence should be addressed. E-mail: liqx@ustc.edu.cn.
[†] University of Science and Technology of China.
[‡] The University of Tokyo.

(1) Henderson, B.; Sibley, W. A. *J. Chem. Phys.* **1971**, *55*, 1276.
(2) Henderson, B.; Kolopus, J. L.; Unruh, W. P. *J. Chem. Phys.* **1971**, *55*, 3519.
(3) Giamello, E.; Paganini, M. C.; Murphy, D. M.; Ferrari, A. M.; Pacchioni, G. *J. Phys. Chem. B* **1997**, *101*, 971.
(4) Ricci, D.; Valentin, C. D.; Pacchioni, G.; Sushko, P. V.; Shluger, A. L.; Giamello, E. *J. Am. Chem. Soc.* **2003**, *125*, 738.
(5) Berger, T.; Sterrer, M.; Diwald, O.; Knözinger, E. *J. Phys. Chem. B* **2004**, *108*, 7280.
(6) Engstrom, H.; Bates, J. B.; Wang, J. C; Abraham, M. M. *Phys. Rev. B* **1980**, *21*, 1520.
(7) González, R.; Pareja, R.; Chen, Y. *Phys. Rev. B* **1992**, *45*, 12730.
(8) González, R.; Chen, Y. *J. Phys.: Condens. Matter* **2002**, *14*, R1143.
(9) Ramírez, R.; Colera, I.; González, R.; Chen, Y.; Kokta, M. R. *Phys. Rev. B* **2004**, *69*, 014302−1.
(10) Chiesa, M.; Paganini, M. C.; Giamello, E.; Murphy, D. M. *Langmuir* **1997**, *13*, 5306.
(11) Ito, T.; Tashiro, T.; Kawasaki, M.; Watanabe, T.; Toi, K.; Kobayashi, H. *J. Phys. Chem.* **1991**, *95*, 4476.
(12) Paganini, M. C.; Chiesa, M.; Martino, P.; Giamello, E.; Garrone, E. *J. Phys. Chem. B* **2003**, *107*, 2575.
(13) Hosono, H.; Abe, Y. *Inorg. Chem.* **1987**, *26*, 1192.
(14) Li, Q. X.; Hayashi, K.; Nishioka, M.; Kashiwagi, H.; Hirano, M.; Torimoto, Y.; Hosono, H.; Sadakata, M. *Appl. Phys. Lett.* **2002**, *80*, 4259.
(15) Li, Q. X.; Hosono, H.; Hirano, M.; Hayashi, K.; Nishioka, M.; Kashiwagi, H.; Torimoto, Y.; Sadakata, M. *Surf. Sci.* **2003**, *527*, 100.
(16) Li, Q. X.; Hayashi, K.; Nishioka, M.; Kashiwagi, H.; Hirano, M.; Torimoto, Y.; Hosono, H.; Sadakata, M. *Jpn. J. Appl. Phys.* **2002**, *41*, L530.
(17) Hayashi, K.; Hirano, M.; Matsuishi, S.; Hosono, H. *J. Am. Chem. Soc.* **2002**, *124*, 738.
(18) Hayashi, K.; Matsuishi, S.; Kamiya, T.; Hirano, M.; Hosono, H. *Nature* **2004**, *419*, 462.
(19) Hayashi, K.; Matsuishi, S.; Ueda, N.; Hirano, M.; Hosono, H. *Chem. Mater.* **2003**, *15*, 1851.
(20) Yang, S.; Konda, J. N.; Hayashi, K.; Hirano, M.; Domen, K.; Hosono, H. *Chem. Mater.* **2004**, *16*, 104.
(21) Matsuishi, S.; Toda, Y.; Miyakawa, M.; Hayashi, K.; Kamiya, T.; Hirano, M.; Tanaka, I.; Hosono, H. *Science* **2003**, *301*, 626.
(22) Toda, Y.; Matsuishi, S.; Hayashi, K.; Ueda, K.; Kamiya, T.; Hirano, M.; Hosono, H. *Adv. Mater.* **2004**, *16*, 685.
(23) Jeevaratnam, J.; Glasser, F. P.; Glasser, L. S. D. *J. Am. Ceram. Soc.* **1964**, *47*, 105.

10.1021/cm0500354 CCC: $30.25 © 2005 American Chemical Society
Published on Web 04/20/2005

$[Ca_{24}Al_{28}O_{64}]^{4+}\cdot 4(e^-)$.[21] A sustainable O^- anion emission current density of $\mu A/cm^2$ level from C12A7-O^- was observed,[14,15] which shows that C12A7-O^- can be used as a good O^- anion storage and emitter. The $[Ca_{24}Al_{28}O_{64}]^{4+}\cdot 4(H^-)$ and $[Ca_{24}Al_{28}O_{64}]^{4+}\cdot 4(e^-)$ crystal can be used as electronic conductor and electride,[18,21−22] and the maximum electron emission current density of 800 $\mu A/cm^2$ can be achieved.

Analogously, O^{2-} in the C12A7 cages can also be substituted by monocharge's diatomic anions AB^-, such as OH^-,[23] to form the derivatives $[Ca_{24}Al_{28}O_{64}]^{4+}\cdot 4(AB^-)$. However, no direct evidence has been reported up to date. In this contribution, we synthesized the C12A7-OH^- material by retreating C12A7-O^- in high-temperature and water vapor environment. On the basis of the investigations of the synthesis material C12A7-OH^-, including the anionic species both on the surface and in the bulk as well as its emission features, we clearly show that the OH^- can substitute for the oxygen anions in the C12A7 crystal, forming an OH^- emission material, i.e., $[Ca_{24}Al_{28}O_{64}]^{4+}\cdot 4(OH^-)$ (C12A7-OH^-). The obtained OH^- emission current density can reach $\mu A/cm^2$ level, which is about 4 orders of magnitude higher than the conventional discharged method.[24] More recently, we also found that this material can be practically used in a high-efficiency one-step synthesis of phenol from benzene or a fast microorganisms' inactivation as a simple OH^- source.

2. Experimental Section

The initial sample (C12A7-O^-) was prepared by the solid-state reaction of $CaCO_3$ and γ-Al_2O_3 under a flowing dry O_2 environment. Powders of $CaCO_3$ and γ-Al_2O_3 were mixed and grained at a molar ratio of $CaCO_3$:γ-Al_2O_3 = 12:7. The powder mixture was pressed to a pellet with a diameter of 15 mm and a thickness of 1.5 mm. After it had been sintered at 1350 °C for 18 h, it was cooled to the room temperature under a flowing dry oxygen atmosphere. To obtain the C12A7-OH^- sample, the C12A7-O^- sample was retreated at 1350 °C for 10 h under a flowing Ar/H_2O mixture (Ar:H_2O = 1:1) atmosphere and then quenched to the room temperature.

For the characteristic measurements, the C12A7 samples are crushed into an average diameter of 40−80 μm. Powder X-ray diffraction (XRD) patterns were recorded on an X'pert Pro Philips diffractometer with a Cu Kα source. The measurement conditions were in the 2θ range of 10−80°, with a step-counting time of 5 s and step size of 0.017° at 298 K. The Fourier-transform IR (FTIR) absorption spectra were measured at 298 K with a Bruker EQUINOX55 FTIR spectrometer with a resolution of ~0.1 cm^{-1}. The samples for FTIR measurements are mixed at a weight ratio of C12A7:KBr = 3:100 and then grained and pressed by a pressure of 300 atm to a pellet with a diameter of 1.0 cm and a thickness of 1.0 mm. Electron paramagnetic resonance measurements were conducted at ~9.1 GHz (X band) using a Bruker ER-200D spectrometer at 77 K. Spin concentrations were determined from the second integral of the spectrum using $CuSO_4\cdot 5H_2O$ as a standard with an error of about 20%.

The emitted anions and electrons from C12A7-OH^- were mass analyzed by a time-of-flight (TOF) mass spectrometer at a background vacuum of about 1×10^{-4} Pa. The experimental apparatus and detailed conditions in this contribution are virtually the same as in the previous works.[14−16] The absolute emission current densities from C12A7-OH^- were observed by a Keithley model 6485 picoammeter. To guarantee an accurate measurement, the samples were replaced when an obvious decrease of the emission intensity was observed, and a calibration was also performed in this work.

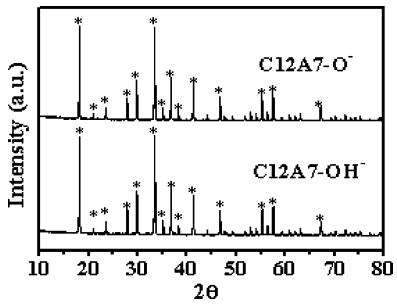

Figure 1. XRD patterns of the C12A7-O^- and C12A7-OH^- samples. By comparison of the peak positions and intensities with the data in JCPDS cards, the peaks marked with an asterisk have been assigned to the structure of C12A7.

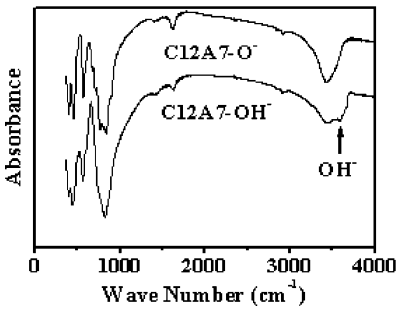

Figure 2. FTIR spectra of C12A7-O^- and C12A7-OH^- samples.

3. Results and Discussion

3.1. Structure of C12A7-OH^-. XRD measurements were employed to investigate the structure difference between C12A7-OH^- and C12A7-O^-. As shown in Figure 1, the peaks that marked by an asterisk have been assigned to the lattice framework of C12A7 by comparing the peak positions and intensities of the XRD pattern with the data in the JCPDS cards. There are nearly no differences between the diffractograms of C12A7-O^- and C12A7-OH^-, which demonstrates that C12A7-OH^- has the same structure of the positively charged lattice framework with C12A7-O^-.

3.2. Anionic Species on the C12A7-OH^- Surface. The presence of OH^- on the C12A7-OH^- surface was observed by the FTIR spectra. Figure 2 shows the FTIR spectra obtained from the C12A7-O^- and C12A7-OH^- samples. The similar absorption both for C12A7-O^- and C12A7-OH^- observed in the spectral region between 450 and 850 cm^{-1} region are attributed to the C12A7 characteristic absorption structures (772.6 cm^{-1}, the Al−O stretching mode in AlO_4 tetrahedral; 400−465 cm^{-1}, the Al−O bending mode in AlO_4 tetrahedral).[25] Even with overlap by a strong 3437-cm^{-1} peak (the water-absorption band of the KBr transparent disk), there is a distinguishable and repeatable peak at 3590 cm^{-1} for the C12A7-OH^- sample. On the other hand, we have not observed the 3590-cm^{-1} band for the C12A7-O^- samples. Because the 3590-cm^{-1} band is close to the frequency ν(O−H$^-$),[26−28] the IR wavelength (in the magnitude of μm)

(24) Schulz, P. A.; Mead, R. D.; Jones, P. L.; Lineberger, W. C. *J. Chem. Phys.* **1982**, *77*, 1153.

(25) Schroeder, R. A.; Lyons, L. L. *J. Inorg. Nucl. Chem.* **1966**, *28*, 1155.

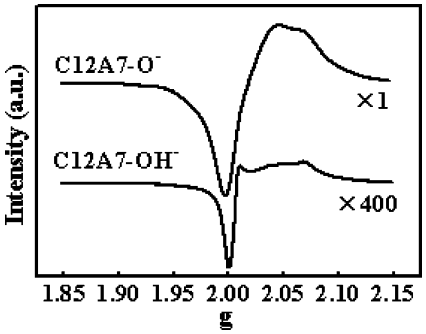

Figure 3. EPR spectra of C12A7-O^- and C12A7-OH^- samples. The symbols ×1 and ×400 in the figure stand for the amplified time of the EPR signal.

is much greater than the C12A7 cages with diameters of about 0.4 nm, which means FTIR maybe could only explore the species on the external surface of the nanoporous structure. Thus, we assign the 3590-cm^{-1} band to the O−H^- stretching vibration on the external surface of C12A7-OH^- cages. The FTIR measurements indicate that OH^- anions appeared on the C12A7-OH^- surface.

3.3. Oxygen Species in C12A7-OH^-. Electron paramagnetic resonance (EPR) measurements were performed to investigate the oxygen species in the bodies of C12A7-O^- and C12A7-OH^-. As shown in Figure 3, the spectra can be decomposed into two components, attributable to the oxygen radicals, O^- ($g_{xx} = g_{yy} = 2.043$ and $g_{zz} = 1.997$) and O_2^- ($g_{xx} = 2.001$, $g_{yy} = 2.010$, and $g_{zz} = 2.070$).[13,17,19−20] By comparison with C12A7-O^-, there are two distinguishing features of the EPR signal for C12A7-OH^-. First, the valley at $g = 2.001$ that corresponds to O_2^- is very sharp, whereas that of C12A7-O^- is rather broad which combines with the O^- signal. Second, there is an obvious and sharp peak at $g_{yy} = 2.010$, which is almost invisible and overlaps with adjacent O^- signals for C12A7-O^-. For C12A7-O^-, the concentrations of O^- and O_2^- are nearly equal by simulating the measured EPR spectra, being about 3.7 and 3.3 × 10^{20} cm^{-3}, respectively. On the other hand, the total concentration of O^- (2.4 × 10^{17} cm^{-3}) and O_2^- (4.6 × 10^{17} cm^{-3}) in C12A7-OH^- sharply decreased to 7 × 10^{17} cm^{-3}, which is only about 0.1% of that in C12A7-O^-. The EPR results show that, after treating the C12A7-O^- sample in the argon atmosphere containing water, nearly all of the O^- and O_2^- anions translate to other species. Even though OH^- anions cannot be directly detected by EPR method, the reformed species in the C12A7-OH^- cages should be attributed to OH^- anions due to OH^- existing on the surface and the desorbed species being almost of OH^- anions (see sections 3.2 and 3.4).

3.4. Emission Features of C12A7-OH^-. The anionic species and electrons emitted from the C12A7-OH^- surface were also investigated by TOF mass spectra. Figure 4 shows a typical mass spectrum at 700 °C with a given extraction field of 400 V/cm. The dominant peak is the mass number of 17, which corresponds to the OH^- anions. And the minor

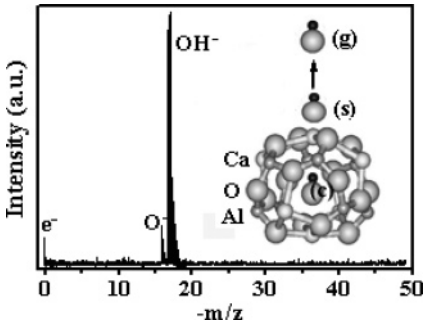

Figure 4. Typical TOF mass spectrum measured for the C12A7-OH^- crystal at 700 °C with a given extraction field of 400 V/cm. The intensity ratio $I(e^-):I(O^-):I(OH^-)$ is about 1:1:16. The insert is a schematic diagram to describe the emission mechanism of OH^- from C12A7-OH^-, where c, s, and g represent the OH^- in the cage, on the sample surface, and in the gas phase.

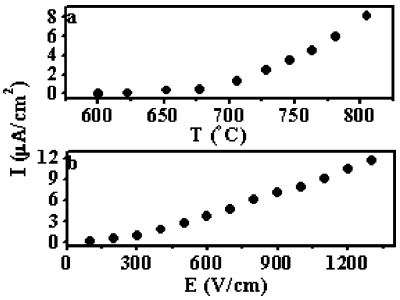

Figure 5. The emission current densities of OH^- measured as the functions of: (a) surface temperature at 800 V/cm and (b) the extraction field at 780 °C.

peak at the mass number of 16 is O^- emitted from the sample. There is also a small peak with the mass number near 0, which is the electron emission. It was found that the anionic species emitted from the C12A7-OH^- sample were quite different from the C12A7-O^- sample. The desorbed species from the C12A7-O^- surface were dominating O^- (∼90%) together with a few electrons (∼10%). On contrast, the main species emitted from the C12A7-OH^- surface were the OH^- anions (about 90%), although weak O^- and electron emission (about 10%) were also observed with an emission intensity ratio of about 1:1. These differences clearly demonstrate that OH^- anions are the major anions in the cages of C12A7-OH^-. The inset of Figure 4 is a schematic diagram to describe the emission mechanism of OH^- from C12A7-OH^-: the OH^- anions in the cages migrate onto the sample surface by field-enhanced thermal diffusion and then are desorbed into the space to form the gas-phase OH^- anions, i.e., OH^- (cage) → OH^- (surface) → OH^- (gas phase). The emission ratio of OH^- to O^- is about 16:1 by calculating the TOF peak areas of OH^- and O^-. The weak O^- emission from C12A7-OH^- would mainly arise from the O^{2-} decomposition process on the surface via the following reaction, O^{2-} (surface) → O^- (surface) + e(surface), and then desorb into space. It would also explain that the emission ratio of O^- to electron is about 1:1.

The absolute emission current density of OH^- was obtained based on the calibration of the total emission current density with the emitted anion distribution. Figure 5a shows OH^- emission current density vs the surface temperature at a given extraction field of 800 V/cm. The emission current density of OH^- strongly depends on the surface temperature

(26) Rosenbaum, N. H.; Owrutsky, J. C.; Tack, L. M.; Saykally, R. J. *J. Chem. Phys.* **1986**, *84*, 5308.
(27) Lee, T. J.; Dateo, C. E. *J. Chem. Phys.* **1997**, *107*, 10373.
(28) Hernández, M. G.; Curulla, D.; Clotet, A.; Illas, F. *J. Chem. Phys.* **2000**, *113*, 364.

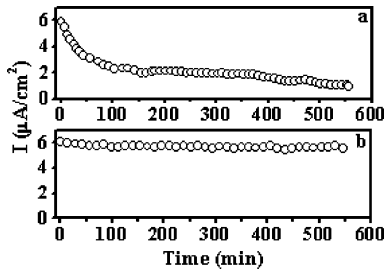

Figure 6. The emission current densities of OH^- measured at 780 °C and 800 V/cm as a function of operating time: (a) without implantation gases and electrons; and (b) with implantation H_2O and electrons on backside of the C12A7-OH^- sample (the implantation gases, H_2O:Ar = 0.15:0.85; pressure, $\sim 4 \times 10^{-2}$ Pa; implantation voltage, −10 V).

and increases about 3 orders of magnitude when the temperature rises from 600 to 800 °C. On the other hand, Figure 5b shows the relationship between the OH^- emission current density and the extraction electronic field at 780 °C. With the increase of extraction field from 100 to 1300 V/cm, the OH^- emission current density remarkably increases from 36 nA/cm^2 to 11.7 μA/ cm^2.

We also have examined the stability of the OH^- emission from C12A7-OH^-. Figure 6a shows the relationship of OH^- emission current density with operating time at 780 °C under a typical extraction field of 800 V/cm. It was found that the initial OH^- intensity of 6 μA/cm^2 decreased to only about 1 μA/cm^2 for 9 h of emission. The decay of OH^- emission is due to the decrease of the OH^- concentration in C12A7-OH^- with increasing emission time. To obtain a sustainable OH^- emission flux, we developed a method of supplying water and electron (by applying a low negative direct current voltage) on the backside of the C12A7-OH^- sample, where OH^- (surface) was supposedly generated by the reaction, H_2O (gas phase) + e^- (surface) → OH^- (surface) + H (surface), and then migrated into the cage of the C12A7-OH^- by the field-enhanced thermal diffusion. As shown in Figure 6b, by continuously supplying H_2O and electrons onto the backside of the C12A7-OH^- sample, the OH^- emission current density was stable at about 5.6 μA/cm^2 with the prolongation of operating time, which means that the C12A7-OH^- crystal can used as a sustainable and stable OH^- source.

3.5. OH^- Formation in C12A7-OH^-. The oxygen species in the cages of C12A7-O^- include O^-, O_2^-, and O^{2-} anions. On the basis of EPR measurements, the concentrations of O^- and O_2^- in C12A7-O^- are obtained, which are about 3.7 and 3.3 $\times$ 10^{20} cm^{-3}, respectively, and the concentration of O^{2-} is estimated to be about 8 $\times$ 10^{20} cm^{-3} by the theoretical maximum monovalent anion concentration in C12A7.[17] We found that the concentrations of O^- and O_2^- in C12A7-OH^- sharply decreased by about 3 orders of magnitude relative to that in C12A7-O^- to about 2.4 and 4.6 $\times$ 10^{17} cm^{-3}, respectively. Moreover, FTIR measurement shows that OH^- anions could appear on the surface of C12A7-OH^-, and TOF results demonstrate that OH^- anions are the main desorbed species. Therefore, beside O^-, O_2^-, and O^{2-} anions, a great deal of OH^- anions should also be caged in C12A7-OH^-. Our results indicated that almost all of O^- and O_2^- are substituted by OH^- with the reactions: (1) H_2O (atmosphere) + O^- (cage) → OH^- (cage) + OH (cage) and (2) H_2O (atmosphere) + O_2^- (cage) → OH^- (cage) + O_2 (cage) + H (cage), when C12A7-O^- was sintered under flowing Ar/H_2O mixture atmosphere. On the other hand, O^{2-} (cage) anions may also react with water to form OH^- (cage) anions by the reaction of H_2O (atmosphere) + O^{2-} (cage) → 2OH^- (cage). Thus, the synthesized C12A7-OH^- material contained rich OH^- anions, at least 7 $\times$ 10^{20} cm^{-3}, which provided us with a new approach to generate high-intensity OH^- anions of the gas phase.

According to our previous work for the C12A7-O^- material, the concentration of cages in the structure is mainly affected by the factors in the preparation procedure of the samples, including the sintering temperature, the sintering pressure, the quenching rate, and the pressure to form a pellet sample. It is also known that the concentration of cages in C12A7 is 7 $\times$ 10^{21} cm^{-3} in our prepared procedure.[17] On the other hand, the concentration of the O^- anions in the C12A7-O^- cages also strongly depends on the preparation conditions of the samples. Particularly, the sintering environment strongly affects the anionic concentration. In this contribution, we only report the results for C12A7-OH^- samples, which were prepared on a typical synthesis condition with the estimated OH^- concentration larger than 7 $\times$ 10^{20} cm^{-3}. To obtain the relationship between the OH^- concentration and the cage concentration, and the optimum condition for the C12A7-OH^- preparation, various preparation conditions should be investigated in our future work. Work toward this goal is in progress.

4. Conclusion

A high-intensity hydroxyl anion emission material C12A7-OH^- is synthesized. The formation of the OH^- anions in C12A7-OH^- is demonstrated by FTIR, EPR, and TOF mass spectra. It is estimated that the OH^- anion concentration is more than 7 $\times$ 10^{20} cm^{-3} in this crystal and that OH^- anions are the dominating anions (90%) emitted from C12A7-OH^-. The sustainable and stable OH^- anions emission in a current density of μA/cm^2 level are obtained, which is strongly dependent on the surface temperature and the extraction field. We expect that the C12A7-OH^- material can be used as an OH^- storage and emitter, and the emitted OH^- anions could be used in chemical synthesis, material modification, and sterilization.

Acknowledgment. The authors thank Ms. Ting Dong and Dr. Jing Tu for the material synthesis. Quan Xin Li thanks the support of the BRP Program and Innovation Program 2002 by the Chinese Academy of Sciences.

CM0500354